CAMBRIDGE
UNIVERSITY PRESS

Article

3D electron diffraction study of terrestrial iron oxide alteration in the Mineo pallasite

Enrico Mugnaioli[1,2] (iD), Azzurra Zucchini[3,4]* (iD), Paola Comodi[3] (iD), Francesco Frondini[3,4] (iD), Luca Bartolucci[3],
Alessandro Di Michele[3] (iD), Paola Sassi[5] (iD) and Mauro Gemmi[2] (iD)

[1]Department of Earth Sciences, University of Pisa, via S. Maria 53, I–56126 Pisa, Italy; [2]Center for Nanotechnology Innovation@NEST, Istituto Italiano di Tecnologia,
Piazza San Silvestro 12, I–56127 Pisa, Italy; [3]Department of Physics and Geology, University of Perugia, via A. Pascoli, I–06123 Perugia, Italy; [4]INFN, Section of
Perugia, via A. Pascoli, I–06123 Perugia, Italy; and [5]Department of Chemistry, Biology and Biotechnology, University of Perugia, via Elce di sotto 8, I–06123 Perugia,
Italy

Abstract

The Mineo pallasite is a relatively poorly known meteorite, which shows interesting features that are not fully understood, such as the occurrence of iron oxide regions bordering both the olivine grain boundaries and the (Fe,Ni) metal. In this study, the Fe oxides have been characterised by Raman spectroscopy, electron microprobe analysis, field emission scanning electron microscopy, transmission electron microscopy (TEM), energy dispersive spectroscopy (EDS) and 3D electron diffraction (3D ED). The combination of TEM–EDS and 3D ED yields a reliable identification of the chemical and crystallographic features of the cryptocrystalline portion of the sample investigated, enabling the Fe-oxide regions to be positively identified as goethite, FeO(OH).

The occurrence of goethite was unambiguously associated with terrestrial alteration, also confirmed by the presence of calcite, detected by TEM-EDS and 3D ED. Goethite contains minor elements such as Na, Si and Ca, probably coming from alumino-silicates in the terrestrial environment, and Ni associated with the (Fe,Ni) metal. The observation of goethite along olivine grain boundaries, as an alteration product of the (Fe,Ni) metal diagenesis, is also very intriguing as it might be related to the (Fe,Ni) metal intruded into the sub-micrometric olivine fragments during pallasite formation. Further work is needed to extensively analyse the texture and composition of olivine/metal boundaries.

Introduction

Pallasites are stony-iron meteorites essentially composed of 35 to 85 vol.% of olivine crystals embedded in a (Fe,Ni) metallic matrix (Weisberg *et al.*, 2006; Boesenberg *et al.*, 2012). Pallasites were originally thought to represent the core–mantle boundary of a differentiated asteroid, subsequently disrupted by impact with a larger body (Yang *et al.*, 2010). As a consequence, the differentiated asteroid was 'dismembered' and olivines from its mantle mixed with the molten (Fe,Ni) from the outer core (Yang *et al.*, 2010). Recently, a more plausible theory invokes the impact of a smaller differentiated body with a partially molten core into a larger differentiated body (∼200 km radius), leading to the intrusion of the liquid (Fe,Ni) from the former into the dunitic mantle of the latter (Tarduno *et al.*, 2012). This theory was suggested because of the strong palaeomagnetic field observed in magnetic inclusions in olivines from Main Group pallasites (Tarduno *et al.*, 2012; Bryson *et al.*, 2015) that is attributed to the presence of a long-lived core dynamo in the differentiated larger body.

Olivines are silicate minerals with the general formula M'M"SiO$_4$ where M = Fe^{2+}, Mg, Mn^{2+}, Ca and Ni. Most rock-forming olivines belong to the Fe–Mg solid-solution series.

The main (Fe,Ni) metal phases in pallasite are iron, the α-(Fe, Ni) metal phase (4–7.5 wt.% Ni), and taenite, the γ-(Fe,Ni) phase (27–65 wt.% Ni). In some cases, a mixture of iron and taenite, called 'plessite', forms in the retained taenite during slow cooling as a consequence of immiscibility between Fe and Ni (Goldstein and Michael, 2006, and references therein). The concentration of minor elements in (Fe,Ni) metal is related to element compatibility and segregation temperature. Thus, (Fe,Ni) metal in pallasites is usually depleted in elements highly compatible with solid metal (Re, Os, Ir, Pt and Ru) and enriched in incompatible elements such as Pd and Au, compared to the early crystallised IIIAB iron meteorites (Mullane *et al.*, 2004).

Minor amounts of sulfides [e.g. troilite FeS], phosphides [e.g. schreibersite (Fe,Ni)$_3$P and barringerite (Fe,Ni)$_2$P], phosphates [e.g. merrillite Ca$_{18}$Na$_2$Mg$_2$(PO$_4$)$_2$, stanfieldite Ca$_3$Mg$_3$(PO$_4$)$_4$ and farringtonite Mg$_3$(PO$_4$)$_2$], chromite FeCr$_2$O$_4$, pyroxene [e.g. orthopyroxenes (Mg,Fe)SiO$_3$] and P-rich olivines (Buseck, 1977) are usually found in pallasites.

Secondary minerals, usually formed in a terrestrial environment either during weathering (e.g. Eggleton, 1984) or post depositional processes (e.g. Gentili *et al.*, 2014), can be found in

altered pallasites. Typical secondary minerals in pallasites are akaganeite β-FeO(OH,Cl), bunsenite NiO, goethite α-FeO(OH), hematite α-Fe$_2$O$_3$, hibbingite γ-Fe$_2$(OH)$_3$Cl, lepidocrocite γ-FeO (OH), maghemite γ-Fe$_2$O$_3$, magnetite Fe$_3$O$_4$ and trevorite NiFe$_2$O$_4$ (Rubin, 1997), which are generally considered to be due to the corrosion of metallic Fe–Ni (Tilley and Bevan, 1998). In addition, olivines can alter in aqueous environments to 'iddingsite', reddish alteration products made of a cryptocrystalline intergrowth of goethite, that can be transformed by dehydration to hematite, and smectite-type phillosilicates (probably saponite, Eggleton, 1984) that can be removed by further alteration.

Mineo pallasite

The Mineo pallasite fell on May 3rd 1826 in Mineo, Sicily, Italy (Baldanza, 1965; Grady, 2000). The only sample in a public collection is owned by the Department of Physics and Geology of the University of Perugia, Italy. The Mineo pallasite was studied in detail for the first time by Zucchini *et al.* (2018). Olivine is forsteritic with Fo < 80. It contains 9–11 wt.% FeO and varying quantities of trace elements, especially Ca (ranging from 62 to 473 ppm) that has a positive correlation with the incompatible elements such as Al, Na, K, Ba and Sr, as well as with the compatible Cr (Zucchini *et al.*, 2018).

The iron–nickel metal is formed primarily as the Fe$_{0.94}$Ni$_{0.06}$ metal alloy phase.

Taenite occurs in plessite structures where a Ni-rich phase with average chemical formula of ~Fe$_{0.83}$Ni$_{0.17}$ is framed by a continuous taenite rim ~10 μm thick. The Ni-rich phase is also present as a droplet-like structure that hosts: (1) a Ni-poor iron matrix (Fe$_{0.94}$Ni$_{0.06}$); (2) taenite (Fe$_{0.81}$Ni$_{0.20}$) as submicrometre- to nano-sized 'droplets'; and (3) a Fe$_{0.60}$Ni$_{0.40}$ high-Ni taenite phase as a rim around the taenite regions (Zucchini *et al.*, 2018).

In addition to the main (Fe,Ni) phases, the metal also contains barringerite and schreibersite. Sulfide phases are rare, represented by only a few grains of troilite (FeS) (Zucchini *et al.*, 2018). The platinum group elements (PGE) and the highly siderophile elements (HSE) show a depletion in the highly compatible elements and an enrichment in Pd and Au with respect to the early crystallised IIIAB irons (Zucchini *et al.*, 2018), following the behaviour of the Main Group pallasites (Mullane *et al.*, 2004) that traces that of the late-crystallised IIIAB irons (medium octahedrites). However, an enrichment in Re, Os and Ir with respect to typical MG pallasites and late-crystallised IIIAB irons has been observed in the Mineo pallasite (Zucchini *et al.*, 2018).

In addition to the major and minor mineral phases usually found in pallasites, regions of iron oxides have been observed. Their origin has not been addressed yet. Possible theories include: (1) the consequence of low-temperature alteration during terrestrial chemical weathering of both the (Fe,Ni) metal previously intruded into the olivine cracks and the olivines themselves; or (2) direct precipitation of Fe oxides from an aqueous solution in the cracks of the highly fractured olivines.

This work

This investigation characterised the Fe oxides in the Mineo pallasite using a multi-analytical approach combining Raman spectroscopy, electron microprobe analysis (EMPA), field emission scanning electron microscopy (FE-SEM), transmission electron microscopy (TEM) and 3D Electron Diffraction (3D ED) (Kolb *et al.*, 2007).

The latter method was crucial for establishing the nature of the Fe oxides and assigning them to goethite. 3D ED consists of the systematic collection of a 3D electron diffraction data set through either a stepwise or continuous rotation of the sample around an arbitrary, non-crystallographic axis. 3D ED delivers single-crystal-like diffraction data from grains of 50–2000 nm in size and is therefore extremely powerful for the identification of minor components in polyphasic mineralogical aggregates (Gemmi *et al.*, 2016). This 3D ED method allows separate structural data to be obtained from all classes of nanometric phases. Moreover, compared to the conventional way of acquiring diffraction data through oriented selected-area electron-diffraction patterns

Fig. 1. (a) Photo of the Mineo pallasite portion owned by the Department of Physics and Geology of the University of Perugia (sample no. Mineo1969.SL3P#002 CNR inventory 213248); (b) isolated olivine single crystal from the Mineo pallasite where a reddish area is observed.
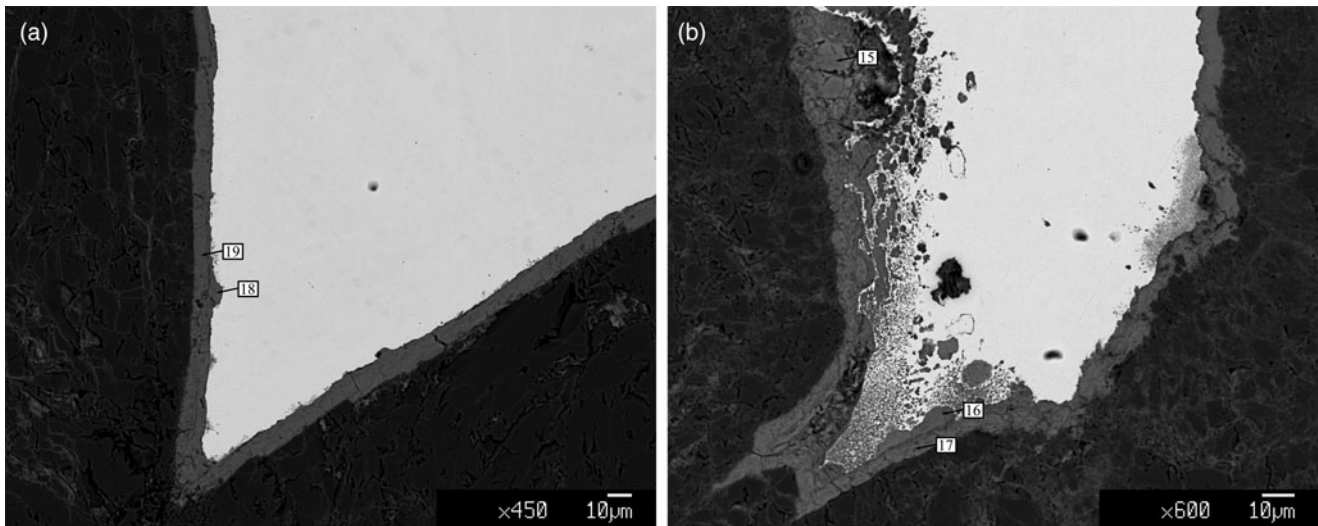
Fig. 2. BSE SEM images of a portion of the Mineo pallasite. Numbers denote sampling points in the iron oxide rim bordering the Fe,Ni metal (Table 1).

(SAED), 3D ED allows a more complete reflection sampling, a reduction of dynamical effects and a decisive acceleration of data acquisition. This results in a reduction of the total electron dose on the sample, which is crucial for beam-sensitive materials. The 3D ED method is currently applied to the structural characterisation of nanocrystalline functional materials (Mugnaioli *et al.*, 2018; Steciuk *et al.*, 2018; Wang *et al.*, 2018), pharmaceuticals (Jones *et al.*, 2018; Brázda *et al.*, 2019) and macromolecules (Nannenga *et al.*, 2014; Xu *et al.*, 2019). A comprehensive review of 3D ED was published recently by Gemmi *et al.* (2019).

In Earth sciences, 3D ED has been used for the structure elucidation of nanoscopic inclusions (Xiong *et al.*, 2020), mineral seeds (Németh *et al.*, 2018), hydrated phases (Mugnaioli *et al.*, 2020a; Krysiak *et al.*, 2021) and modulated systems (Lanza *et al.*, 2019; Steciuk *et al.*, 2020), even when characterised by very large asymmetric units (Rozhdestvenskaya *et al.*, 2010; Mugnaioli *et al.*, 2020b). 3D ED has been applied to geological samples in different contexts (Mugnaioli and Gemmi, 2018), and in particular for the characterisation of meteorites (Pignatelli *et al.*, 2017, 2018; Suttle *et al.*, 2021), impactites (Campanale *et al.*, 2021), cryptocrystalline oxides (Koch-Müller *et al.*, 2014) and hydroxides (Viti *et al.*, 2016).

Experimental methods

Meteorite sampling

The available portion of the Mineo pallasite is shown in Fig. 1a and the single crystal of olivine with reddish surfaces chosen for the current study in Fig. 1b, that was extracted together with micrometric to nanometric reddish aggregates sampled from the Fe-oxide regions.

Field emission – scanning electron microscopy (FE–SEM) and electron microprobe analysis (EMPA)

High-resolution back-scattered electron (BSE) FE–SEM images were obtained by a field-emission-gun electron scanning microscope (LEO 1525) and a ZEISS AsB (angle selective back-scattered) Detector, at the Department of Physics and Geology

of the University of Perugia, coupled with a Bruker Quantax EDS operating at 15 kV. Chemical analyses of the Fe-oxide areas were performed at the "Ardito Desio" Earth Sciences Department of the University of Milan using a JEOL 8200 Super Probe operating at 15kV acceleration voltage and 5 nA current. The instrument is equipped with five WDS (wavelength dispersive) and one EDS (energy dispersive) spectrometers. In the Fe-oxide areas, five points were analysed (Fig. 2).

Raman spectroscopic analyses

Raman spectroscopic analyses of the olivine single crystal were performed at the Department of Chemistry, Biology and Biotechnology, University of Perugia. The analytical set up consisted of: back-scattering illumination and collection of the scattered light through an Olympus confocal microscope MOD BX40 (50× objective); 532 nm excitation from the solid-state laser Oxxius LMX (laser power on the sample 45 mW); 1024×256 CCD array Syncerity by Horiba – Jobin Yvon to detect the scattered light. A spectral resolution of ~4 cm^{-1} was achieved
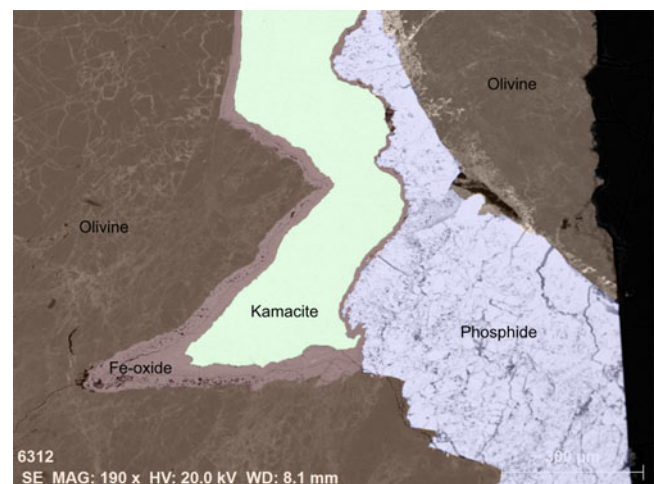

Fig. 3. BSE FE-SEM image of a portion of the Mineo pallasite. The BSE image was coloured according to the mineral assemblage shown by qualitative EDS investigation.

with a 1800 lines mm^{-1} grating of an iHR320 imaging spectrometer. Spectral measurements were made with continuous scans in the range 200–1800 cm^{-1}, exposure times in the range 30–60 s, and 10 accumulations. The spectrometer was calibrated using the Raman lines of WO_3 powder. The collected Raman spectra were baseline-corrected to eliminate the background by using the *Peak Analyzer* routine of *Origin 8.0* software (OriginLab Corporation, Northampton, MA, USA).
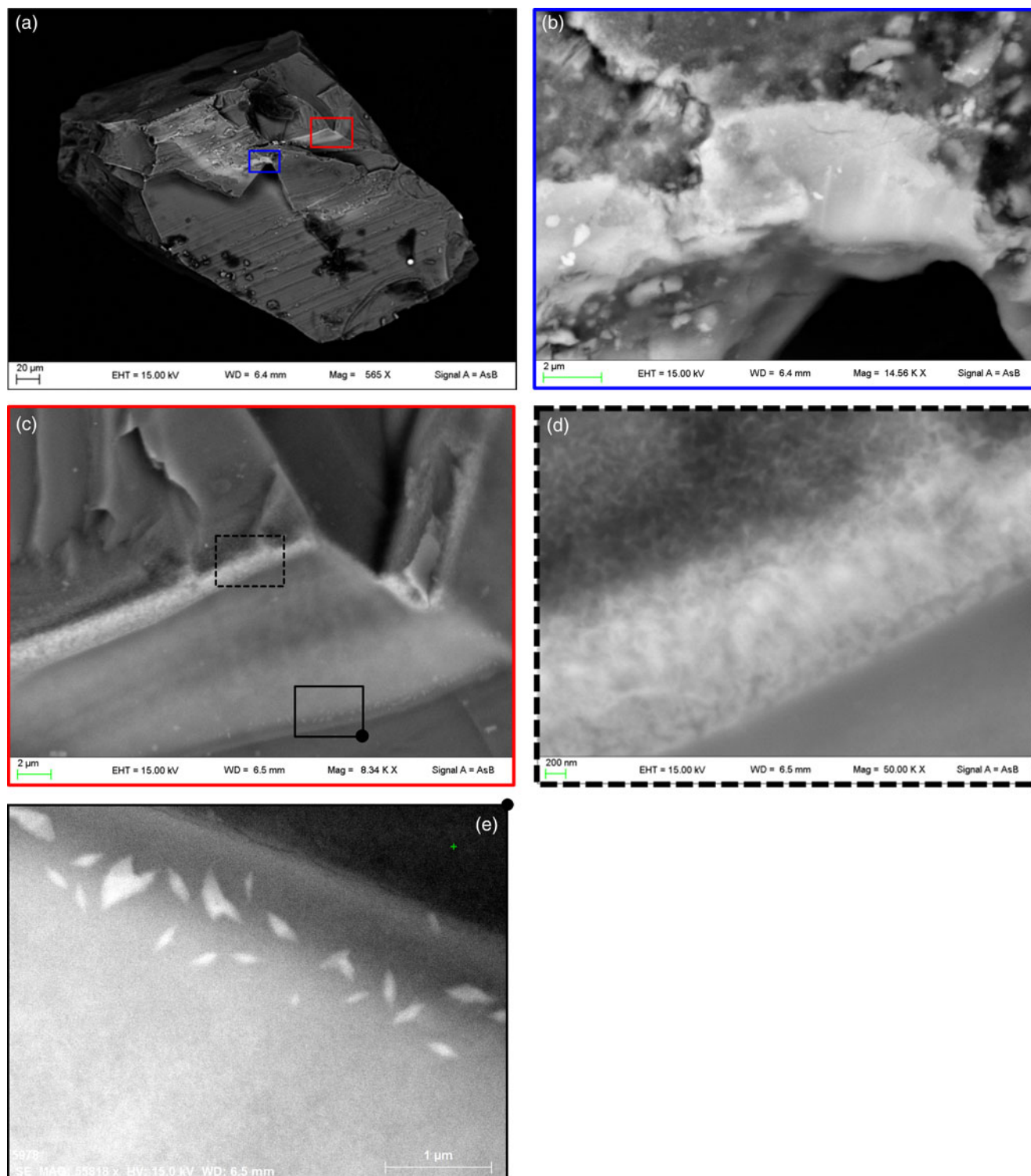

Fig. 4. BSE FE-SEM images of the olivine single crystal isolated from the Mineo pallasite. (a) The whole single crystal. Blue and red rectangles show the location of areas of high Fe concentration enlarged in (b) and (c), respectively. Dashed black and solid boxes in (c) show the areas enlarged in (d) and (e, rotated 180°), respectively.

Table 1. Compositions (wt.%) from EMPA of Fe oxide at location points 15 to 19 (Fig. 2). Analytical precision is in accordance with the last decimal place.

Point	15	16	17	18	19
Na_2O	0.51	0.42	0.21	0.43	0.27
TiO_2	-	-	0.01	-	-
MnO	0.02	-	0.03	0.03	-
K_2O	0.08	0.02	0.05	0.04	0.05
MgO	5.2	3.5	4.6	3.5	4.5
SiO_2	0.6	0.8	2.1	0.1	1.6
Cr_2O_3	-	0.03	-	-	-
FeO	71.0	72.7	66.7	64.3	61.6
CaO	1.06	0.37	0.43	0.19	0.28
Al_2O_3	-	0.03	-	0.02	0.02
NiO	4.85	2.78	6.26	5.31	4.71
Total	83.4	80.6	80.4	74.0	73.0

'-' not detected

Transmission electron microscopy (TEM) and 3D electron diffraction (3D ED)

A few small portions of the Fe-rich areas in the Mineo pallasite, such as the region bordering the olivine to iron interface in Fig. 2, were crushed to reach the optimal grain dimensions needed for the TEM and 3D ED analysis. 3D ED measurements (Mugnaioli and Gemmi, 2018; Gemmi *et al.*, 2019) were performed at the Center for Nanotechnology Innovation (NEST, Istituto Italiano di Tecnologia, Pisa, Italy) by a Zeiss Libra TEM operating at 120 kV and equipped with a LaB_6 source and a Bruker EDS detector XFlash6T-60. 3D ED acquisitions were done in STEM mode after defocusing the beam in order to have pseudo-parallel illumination on the sample. A beam size of ∼150 nm in diameter was obtained by inserting a 5 μm C2 condenser aperture. Conventional ED and 3D ED data, the latter acquired in steady steps of 1°, were recorded by an ASI Timepix detector and analysed by *ADT3D* software (Kolb *et al.*, 2011) and in-house developed *MATLAB* routines.

Results

Chemical analyses

The FE-SEM and EDS analyses show the occurrence of iron oxides bordering the (Fe,Ni) metals, mainly iron (Fig. 3), confirming the results from Zucchini *et al.* (2018).

Iron oxide was also observed as reddish areas on the olivine single crystals (Fig. 1b) appearing as light contrast halos and bands, related to the concentration of atoms with a high atomic number such as Fe, as shown by FE-SEM EDS analyses (Fig. 4). The white bands observed on the surface of the olivine crystal were found to be formed by aggregates of Fe-rich nanometric particles (Fig. 4d). In some areas, structures resembling exsolution lamellae were also observed (Fig. 4e).

Electron microprobe analyses within the Fe-oxide areas (Fig. 2) showed the occurrence of high Fe contents, followed by Ni and Mg. Minor elements are also detected, mainly Na, Si and Ca in order of abundance (Table 1).

Raman spectroscopic results on the Fe-oxide phases are shown in Fig. 5. Contribution from both Fe-oxide phases and olivine were collected and the contribution of Fe-oxides was isolated by
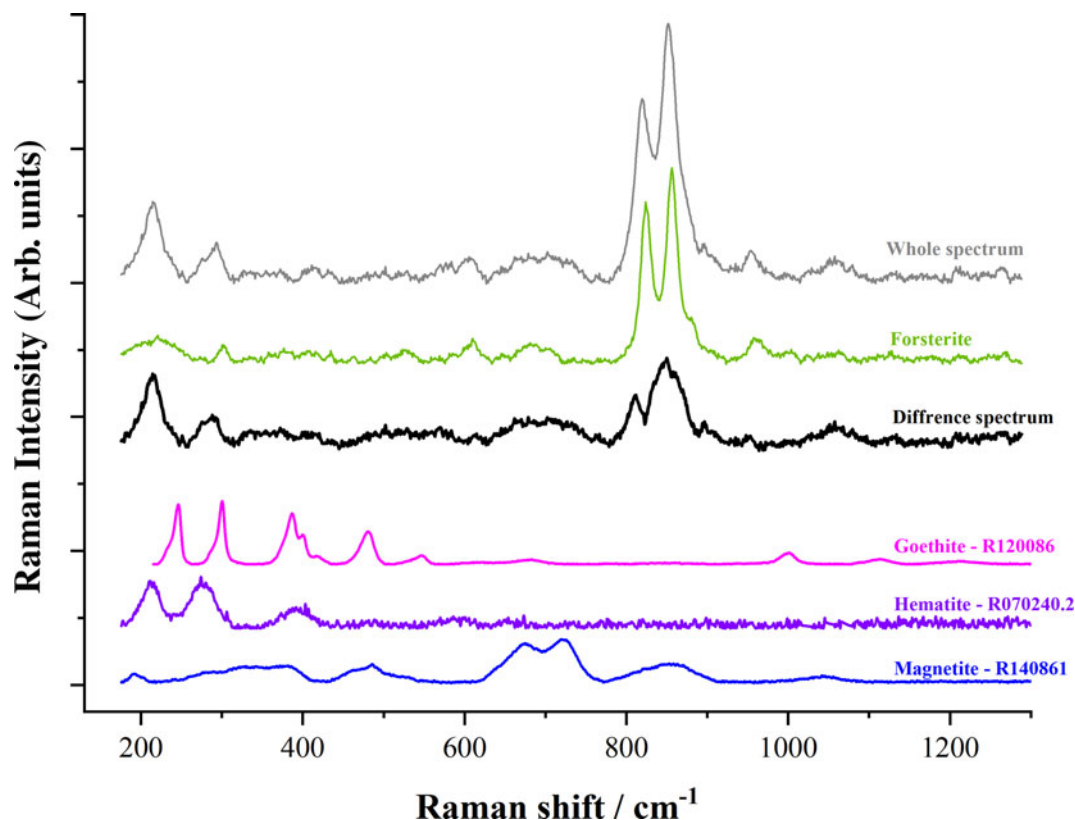

Fig. 5. Raman analyses on the olivine single crystal from the Mineo pallasite. Collected data on the Fe-oxide-rich phase ('whole spectrum' in grey) were processed by subtracting the olivine contribution (collected green spectrum). The difference spectrum is given in black. The compared phases are shown: goethite (pink), hematite (purple) and magnetite (blue). Reference codes of the RRUFF database (Lafuente *et al.*, 2015) for the compared spectra are shown in the figure.

subtracting olivine signals from the whole spectrum. The main forsteritic signals are still quite evident as two main peaks around 800 cm^{-1}; however, the relative intensities of these two are different in the whole spectrum compared to what is observed for the forsterite spectrum. We performed the subtraction in order not to have a negative peak in the 200–1300 cm^{-1} range and obtained a residual intensity particularly in the 200–300 and 800–900 cm^{-1} regions. The broad feature at 800–900 cm^{-1} could be due to the different forsterite structures of the two samples, i.e. a reduced crystallinity of this phase in the Mineo pallasite, compared with the olivine single crystal. The peaks at 212.5 and 282.2 cm^{-1} might be attributed to hematite; whereas, the features in the range 625–770 cm^{-1} might be related to magnetite (Hanesch, 2009). The goethite spectrum was also reported for comparison. However, the features attributed to the Fe oxides (212.5 and 282.2 cm^{-1}) seems to have shorter wavelengths compared to goethite.

TEM and 3D ED analysis

The mineralogical assignment of alteration phases by conventional analytical techniques was inconclusive due to the sub-micrometric dimension and polycrystallinity of the Fe-rich regions. In fact, preliminary single-crystal X-ray diffraction analysis performed on the isolated single crystal showed no diffraction peak different from those of olivine. The reasons for this behaviour might be either the very low crystallinity or the sub-micrometric dimensions of the high-Fe phases.

Therefore, TEM and 3D ED analyses were performed on these areas to further elucidate their textures and crystal structure. Grains were isolated from the Fe-rich regions within the olivine single crystal and from the Fe-rich areas of the meteorite. The powdered sample was first analysed by TEM-EDS, which allowed identification of particles made only of Fe oxides. Most of the other particles were olivine fragments and, unexpectedly, CaCO$_3$ crystals.

The isolated Fe-oxide grains in Fig. 6 are nano-polycrystalline aggregates. Most crystals are nanometres in size and too small and aggregated to perform 3D ED analysis, but occasionally it was possible to find coherent crystalline areas of some hundreds of nanometres in width. Only when a fragment hosted a dominant coherent crystalline area of at least 100 nanometers in size, could a unit cell be defined (Fig. 7). Spurious extra reflections, with an intensity sometimes comparable with the dominant crystalline area, were always present and originated from surrounding Fe-oxide crystals. Automatic routines for cell-parameter determination systematically failed and a cell consistent with most of the collected reflections could be obtained only after a careful inspection of the 3D reconstructed data sets. In all cases, we observed a unit cell with parameters $a = 4.8(1)$ Å, $b = 10.0(2)$ Å, $c = 2.8(1)$ Å and $\alpha \approx \beta \approx \gamma \approx 90°$. In addition, extinction rules consistent with space group Pbnm were observed. This evidence points to the orthorhombic structure of goethite FeO(OH).

In order to verify that this phase identification could be extended to the more cryptocrystalline portion of Fe-oxide aggregates, several ring diffraction patterns (conceptually comparable with powder diffraction) were collected from polycrystalline Fe-oxide areas. For these measurements, the beam was enlarged
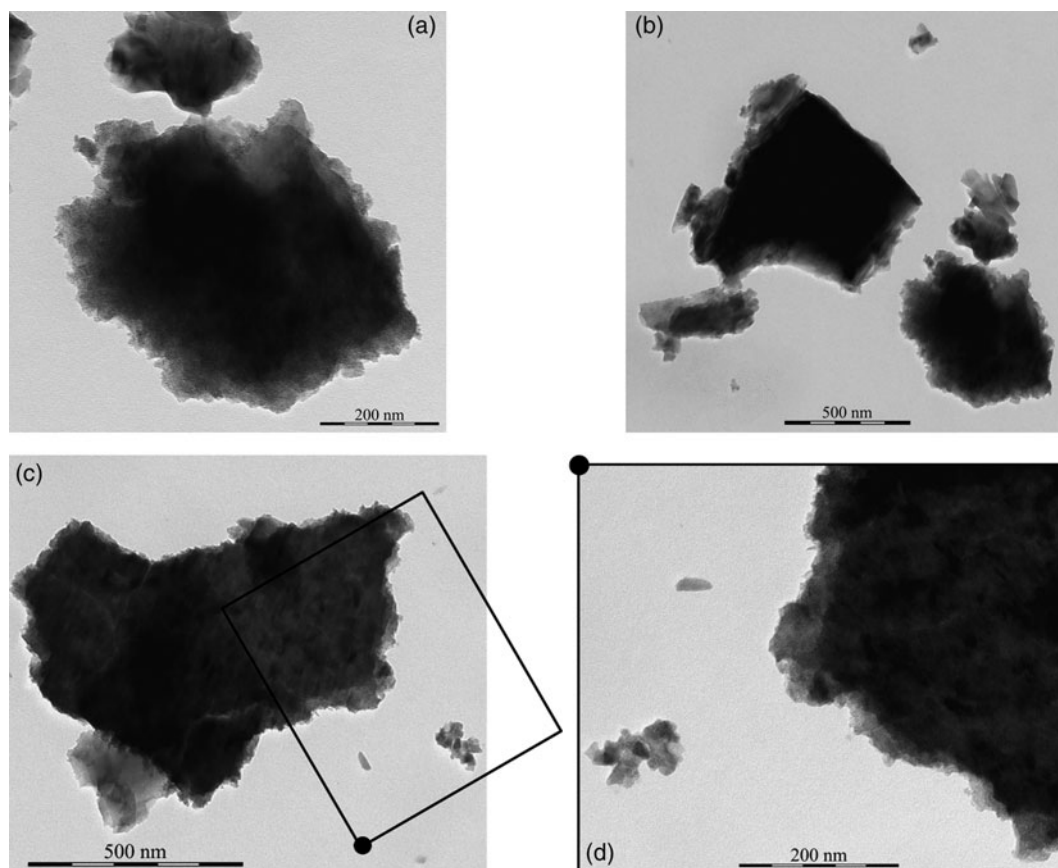

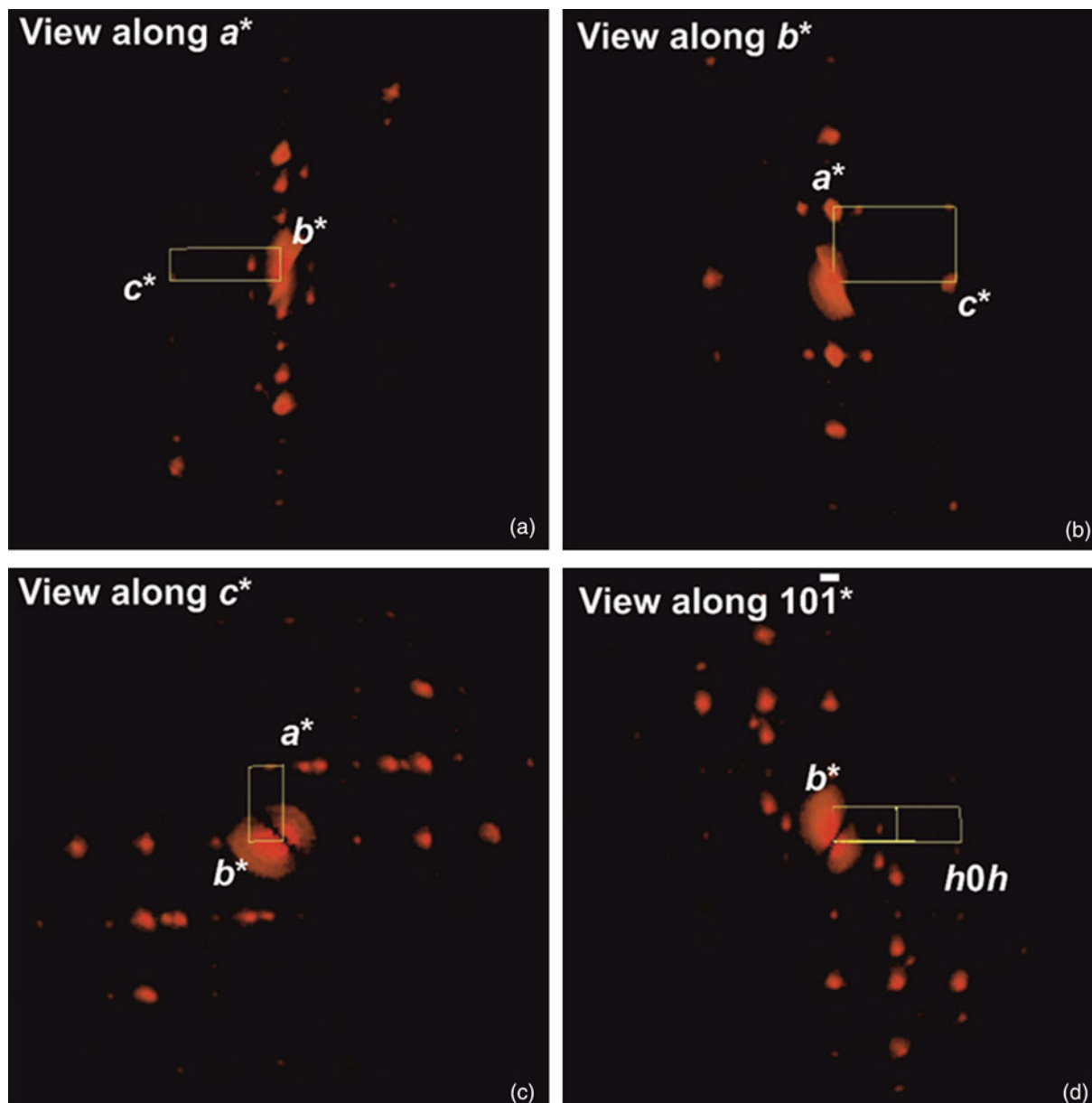**Fig. 6.** TEM images of different nano-sized Fe-oxide grains (a, b, c). In (d) a zoomed portion of (c) is shown.

Fig. 7. Reconstructed 3D ED data for a mostly coherent Fe-oxide grain, consistent with goethite lattice. (a) View along a*; (b) view along b*; (c) view along c*, showing missing reflections $0kl : k = 2n + 1$, consistent with the (100) *b*-glide plane of goethite; and (d) view along $10\bar{1}^*$, showing missing reflections $h0l$: $h + l = 2n + 1$, consistent with the (010) *n*-glide plane of goethite. An important fraction of reflections does not belong to the main goethite domain, whose unit cell is sketched in yellow. Cell vector projections are labelled in white. The number of spurious reflections is emphasised by the fact that reflections belonging to the main goethite domain overlay in projection. One should consider that these images are not conventional 2D electron diffraction patterns, but projections of the whole 3D diffraction reconstruction.

to ∼500 nm to sample more crystallites and obtain a better intensity distribution (Fig. 8). The diffraction rings were consistently indexed with typical goethite interplanar spaces (see for example RRUFF ID R050142; Lafuente *et al.*, 2015).

Finally, 3D ED was performed on $CaCO_3$ crystals with sizes <100 nm, allowing identification of the cell parameters for calcite. This mineral generally appears in close association with goethite aggregates.

Discussion

The results from EMPA gave an average composition of the Fe- and Ni-oxides of 67±4 and 5±1 wt.%, respectively, and

detected other minor elements as Mg, Si, Ca and Na. The low totals might be due to the presence of undetectable chemical species, such as OH and water. As regards the Raman analyses, the Fe-oxide grains were attributed to hematite, with a slight magnetite contribution. In contrast, coupling 3D ED and TEM-EDS analyses, we were able to unequivocally assign the observed Fe-oxide grains to goethite, confirming the supposed presence of hydrated Fe oxides suggested by the EMPA. The reason for the discrepant results from the Raman analysis may be the alteration of goethite to hematite by laser-induced effects, as shown by Seifert *et al.* (2010), giving rise to aggregates of hematite with possible magnetite contributions, as observed in Fig. 5.
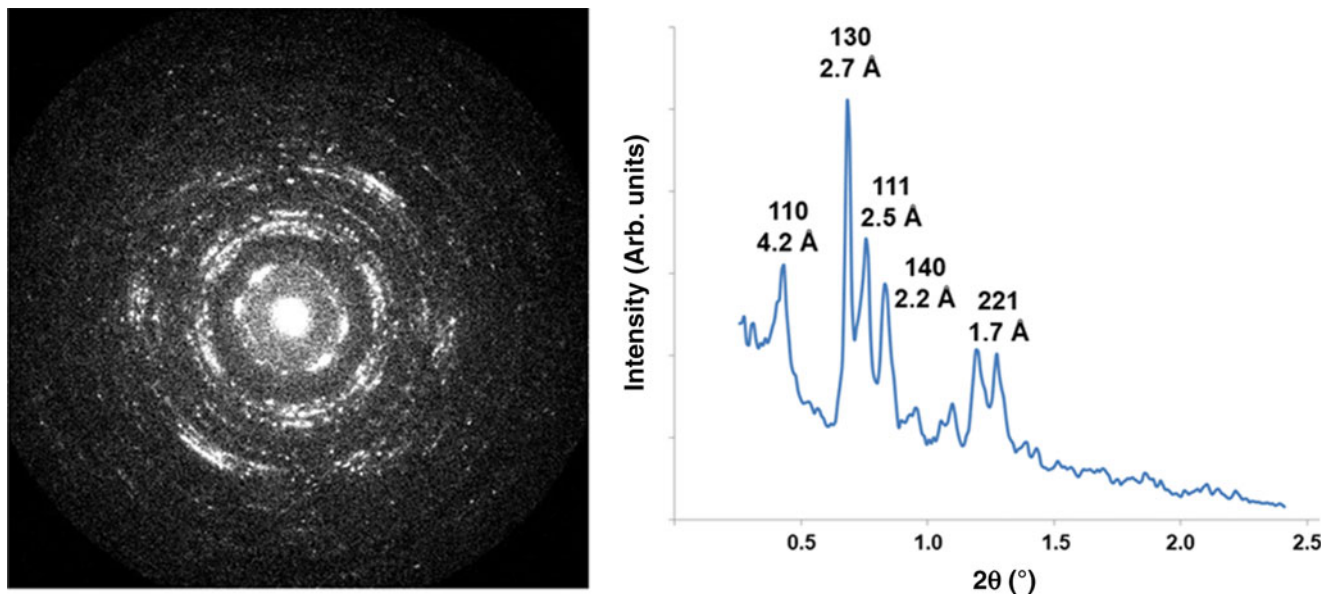
Fig. 8. Electron diffraction rings of a polycrystalline Fe-oxide aggregate, showing interplanar distances consistent with goethite. The plot on the right was obtained by an intensity integration of the rings. Measured interplanar distances and related indexes are indicated.

The occurrence of goethite in the mineral assemblage of the Mineo pallasite is reasonably assigned to terrestrial alteration, also confirmed by the presence of calcite, which was probably precipitated from circulating water.

The EMPA on the goethite areas showed the presence of minor elements, such as Ni, Mg, Si, Ca and Na, that might be due either to their incorporation into the Fe-oxide crystal structure, or to the presence of accessory minerals. The former hypothesis suits Ni very well, as it is a major element of the (Fe,Ni) metal, however it does not explain the occurrence of the other chemical species that could be related to the presence of other mineralogical components, probably coming from interactions with the terrestrial environment. The likely occurrence of cryptocrystalline mineral associations, such as iddingsite, resulting from olivine alteration, cannot be excluded. However, on the one hand, the observed minor elements occurrence that cannot be related to smectite-type phyllosilicates, and, on the other hand, the textural occurrence of the goethite areas mainly bordering on the (Fe,Ni) metal (Fig. 3), are good reasons to attribute goethite to oxidation of the metallic component.

Goethite was also observed on the grain boundaries between the fragmented olivines where the (Fe,Ni) metal probably intruded during pallasite formation, as shown by the reddish areas on the isolated single crystal in Fig. 1b. This observation is not common for pallasite, where olivines usually occur as macrocrystals with size ranges from a few hundreds of micrometres to a few centimetres (Scott, 1977). Thus, further analyses of major-, minor- and trace-elements distribution in olivines, as well as on the fragmentation of olivines and other constituent phases in the Mineo pallasite, are needed.

This study shows how for polyphasic and cryptocrystalline samples, even simple mineralogical identification can benefit strongly from TEM methods. In particular, the combination of TEM-EDS and 3D ED can deliver chemical and crystallographic information on the same nanometric portion of the sample, allowing recognition of any mineral species without ambiguities even for low-symmetry systems. This protocol may become a routine path for discriminating and validating new nanometric mineral species, and possibly will expand our understanding of geological and planetary phenomena.

Conclusions

The detailed characterisation of Fe-oxide alteration in Mineo pallasite shows once more how the combination of TEM-EDS and 3D ED allows unambiguous mineral phase identification at the nanoscale. Chemical and structural information can be retrieved from single nano-grains, even when these are minor constituents of a polycrystalline aggregate. This is an obvious advantage when compared with spectroscopic and X-ray diffraction methods that deliver a global signal from the whole ensemble of material. Future applications of such an approach look especially promising for rocks forming in a short time and in unequilibrated conditions, such as alteration bands, fault mirrors, impact rocks and meteorites.

Results of the present work show that the Fe-oxide regions are goethite, derived from chemical weathering in a terrestrial environment of the (Fe,Ni) metal that possibly also intruded on the grain boundaries between the fragmented olivines during pallasite formation.

References

Baldanza B. (1965) Italian meteorites. *Mineralogical Magazine*, **35**, 214–232.

Boesenberg J.S., Delaney G.S. and Hewins R.H.J. (2012) A petrological and chemical reexamination of Main Group pallasite formation. *Geochimica et Cosmochimica Acta*, **89**, 134–158.

Brázda P., Palatinus L. and Babor M. (2019) Electron diffraction determines molecular absolute configuration in a pharmaceutical nanocrystal. *Science*, **364**, 667–669.

Bryson J.F.J., Nichols C.I.O., Herrero-Albillos J., Kronast F., Kasama T., Alimadadi H., van der Laan G., Nimmo F. and Harrison R.J. (2015) Long-lived magnetism from solidification-driven convection on the pallasite parent body. *Nature*, **517**, 472–475.

Buseck P.R. (1977) Pallasite meteorites mineralogy, petrology and geochemistry. *Geochimica et Cosmochimica Acta*, **41**, 711–740.

Campanale F., Mugnaioli E., Gemmi M. and Folco L. (2021) The formation of impact coesite. *Scientific Reports*, **11**, 16011.

Eggleton R.A. (1984) Formation of iddingsite rims on olivine: a transmission electron microscope study. *Clays and Clay Minerals*, **32**, 1–11.

Gemmi M., Merlini M., Palatinus L., Fumagalli P. and Hanfland M (2016) Electron diffraction determination of 11.5 Å and HySo structures: Candidate water carriers to the Upper Mantle. *American Mineralogist*, **101**, 2645–2654.

Gemmi M., Mugnaioli E., Gorelik T.E., Kolb U., Palatinus L., Boullay P., Hovmöller S. and Abrahams JP (2019) 3D Electron Diffraction: The Nanocrystallography Revolution. *ACS Central Science*, **5**, 1315–1329.

Gentili S., Comodi P., Nazzareni S. and Zucchini A. (2014) The Orvieto-Bagnoregio Ignimbrite: pyroxene crystal-chemistry and bulk phase composition of pyroclastic deposits, a tool to identify syn-and post-depositional processes. *European Journal of Mineralogy*, **26**, 743–756.

Goldstein J.I. and Michael J.R. (2006) The formation of plessite in meteoritic metal. *Meteoritics & Planetary Science*, **41**, 553–570.

Grady M.M. (2000) *Catalogue of Meteorites Reference Book*, 5th Ed. Cambridge University Press, Cambridge, UK, 696 pp.

Hanesch M. (2009) Raman spectroscopy of iron oxides and (oxy)hydroxides at low laser power and possible applications in environmental magnetic studies. *Geophysical Journal International*, **177**, 941–948.

Jones C.G., Martynowycz M.W., Hattne J., Fulton T.J., Stoltz B.M., Rodriguez J.A., Nelson H.M. and Gonen T (2018) The CryoEM method MicroED as a powerful tool for small molecule structure determination. *ACS Central Science*, **4**, 1587–1592.

Koch-Müller M., Mugnaioli E., Rhede D., Speziale S., Kolb U. and Wirth R. (2014) Synthesis of a quenchable high-pressure form of magnetite (h-Fe_3O_4) with composition $^{Fe1}(Fe^{2+}_{0.75}Mg_{0.26})^{Fe2}(Fe^{3+}_{0.70}Cr_{0.15}Al_{0.11}Si_{0.04})_2O_4$. *American Mineralogist*, **99**, 2405–2415.

Kolb U., Gorelik T., Kübel C., Otten M.T. and Hubert D (2007) Towards automated diffraction tomography: Part I—Data acquisition. *Ultramicroscopy*, **107**, 507–513.

Kolb U., Mugnaioli E. and Gorelik T.E. (2011) Automated electron diffraction tomography – a new tool for nano crystal structure analysis. *Crystal Research and Technology*, **46**, 542–554.

Krysiak Y., Maslyk M., Nádia Silva B., Plana-Ruiz S., Moura H.M., Munsignatti E.O., Vaiss V.S., Kolb U., Tremel W., Palatinus L., Amaral Leitão A., Marler B. and Pastore H.O. (2021) The elusive structure of magadiite, solved by 3D electron diffraction and model building. *Chemistry of Materials*, **33**, 3207–3219.

Lafuente B., Downs R.T., Yang H. and Stone N (2015) *The Power of Databases: the RRUFF project* Pp. 1–30 in: *Highlights in Mineralogical Crystallography* (T. Armbruster and R.M. Danisi, editors). W. De Gruyter, Berlin.

Lanza A.E., Gemmi M., Bindi L., Mugnaioli E. and Paar W.H. (2019) Daliranite, $PbHgAs_2S_5$: determination of the incommensurately modulated structure and revision of the chemical formula. *Acta Crystallographica,* **B75**, 711–716.

Mugnaioli E. and Gemmi M. (2018) Single-crystal analysis of nanodomains by electron diffraction tomography: mineralogy at the order-disorder borderline. *Zeitschrift für Kristallographie*, **233**, 163–178.

Mugnaioli E., Gemmi M., Tu R., David J., Bertoni G., Gaspari R., De Trizio L. and Manna L. (2018) *Ab initio* structure determination of $Cu_{2−x}Te$ plasmonic nanocrystals by precession-assisted electron diffraction tomography and HAADF-STEM imaging. *Inorganic Chemistry*, **57**, 10241–10248.

Mugnaioli E., Lanza A.E., Bortolozzi G., Righi L., Merlini M., Cappello V., Marini L., Athanassiou A. and Gemmi M. (2020a) Electron diffraction on flash-frozen cowlesite reveals the structure of the first two-dimensional natural zeolite. *ACS Central Science*, **6**, 1578–1586.

Mugnaioli E., Bonaccorsi E., Lanza A.E., Elkaim E., Diez-Gómez V., Sobrados I., Gemmi M. and Gregorkiewitz M. (2020b) The structure of kaliophilite $KAlSiO_4$, a long-lasting crystallographic problem. *IUCrJ*, **7**, 1070–1083.

Mullane E., Alard O., Gounelle M. and Russella S.S. (2004) Laser ablation ICP-MS study of IIIAB irons and pallasites: Constraints on the behaviour of highly siderophile elements during and after planetesimal core formation. *Chemical Geology*, **208**, 5–28.

Nannenga B.L., Shi D., Leslie A.G.W. and Gonen T. (2014) High-resolution structure determination by continuous-rotation data collection in MicroED. *Nature Methods*, **11**, 927–931.

Németh P., Mugnaioli E., Gemmi M., Czuppon G., Demény A. and Spötl C. (2018) A nanocrystalline monoclinic $CaCO_3$ precursor of metastable aragonite. *Sciences Advances*, **4**, eaau6178.

Pignatelli I., Marrocchi Y., Mugnaioli E., Bourdelle F. and Gounelle M. (2017) Mineralogical, crystallographic and redox features of the earliest stages of fluid alteration in CM chondrites. *Geochimica et Cosmochimica Acta*, **209**, 106–122.

Pignatelli I., Mugnaioli E. and Marrocchi Y. (2018) Cronstedtite polytypes in the Paris meteorite. *European Journal of Mineralogy*, **30**, 349–354.

Rozhdestvenskaya I., Mugnaioli E., Czank M., Depmeier W., Kolb U., Reinholdt A. and Weirich T. (2010) The structure of charoite, $(K,Sr,Ba,Mn)_{15−16}(Ca, Na)_{32}[(Si_{70}(O,OH)_{180})](OH,F)_{4.0} \cdot nH_2O$, solved by conventional and automated electron diffraction. *Mineralogical Magazine*, **74**, 159–177.

Rubin A.E. (1997) Mineralogy of meteorite groups. *Meteoritics & Planetary Science*, **32**, 231–247.

Scott R.D. (1977) Formation of olivine-metal textures in pallasite meteorites. *Geochimica et Cosmochimica Acta*, **6**, 693–710.

Seifert W., Thomas R., Rhede D. and Forster H.-J. (2010) Origin of coexisting wustite, Mg–Fe and REE phosphate minerals in graphite-bearing fluorapatite from the Rumburk granite. *European Journal of Mineralogy*, **22**, 495–507.

Steciuk G., Barrier N., Pautrat A. and Boullay P. (2018) Stairlike aurivillius phases in the pseudobinary $Bi_5Nb_3O_{15}−ABi_2Nb_2O_9$ (A = Ba and Sr) System: A comprehensive analysis using superspace group formalism. *Inorganic Chemistry*, **57**, 3107–3115.

Steciuk G., Škoda R., Rohlíček J. and Plášil J. (2020) Crystal structure of the uranyl–molybdate mineral calcurmolite $Ca[(UO_2)_3(MoO_4)_2(OH)_4](H_2O)_{\sim 5.0}$: insights from a precession electron-diffraction tomography study. *Journal of Geosciences*, **65**, 15–25.

Suttle M.D., Folco L., Genge M.J., Franchi I. A., Campanale F., Mugnaioli E. and Zhao X. (2021) The aqueous alteration of GEMS-like amorphous silicate in a chondritic micrometeorite by Antarctic water. *Geochimica et Cosmochimica Acta*, **293**, 399–421.

Tarduno J.A., Cottrell R.D., Nimmo F., Hopkins J., Voronov J., Erickson A., Blackman E., Scott E.R.D. and McKinley R. (2012) Evidence for a dynamo in the main group pallasite parent body. *Science*, **338**, 939–942.

Tilley D. and Bevan A. (1998) The prolonged weathering of iron and stony-iron meteorite and their anomalous contribution to the Australian regolith. Pp. 77–88 in *New Approaches to an Old Continent, Proceedings of the 3rd Australian Regolith Conference (Kalgoorlie, Canberra)* (G. Taylor and C.F. Pain, editors). Perth: Cooperative Research Centre for Landscape Evolution & Mineral Exploration (CRC LEME).

Viti C., Brogi A., Liotta D., Mugnaioli E., Spiess R., Dini A., Zucchi M. and Vannuccini G. (2016) Seismic slip recorded in tourmaline fault mirrors from Elba Island (Italy). *Journal of Structural Geology*, **86**, 1–12.

Wang B., Rhauderwiek T., Inge A.K., Xu H., Yang T., Huang Z., Stock N. and Zou X. (2018) A porous cobalt tetraphosphonate metal–organic framework: accurate structure and guest molecule location determined by continuous-rotation electron diffraction. *Chemistry – A European Journal*, **24**, 17429–7433.

Weisberg M.K., McCoy T.J. and Krot A.N. (2006) Systematics and evaluation of meteorite classification. Pp. 19–52 in: *Meteorites and the Early Solar System II* (D.S. Lauretta and H.Y. McSween Jr., editors). University of Arizona Press, Tucson, Arizona, USA.

Xiong F., Xu X., Mugnaioli E., Gemmi M., Wirth R., Grew E.S., Robinson P.T. and Yang J. (2020) Two new minerals, badengzhuite, TiP, and zhiqinite, TiSi$_2$, from the Cr–11 chromitite orebody, Luobusa ophiolite, Tibet, China: is this evidence for super-reduced mantle-derived fluids? *European Journal of Mineralogy*, **32**, 557–574.

Xu H., Lebrette H., Clabbers M.T.B., Zhao J., Griese J.J., Zou X. and Högbom M (2019) Solving a new R2lox protein structure by microcrystal electron diffraction. *Science Advances*, **5**, eaax4621.

Yang J., Goldstein J.I. and Scott E.R.D. (2010) Main-group pallasites: Thermal history, relationship to IIIAB irons, and origin. *Geochimica et Cosmochimica Acta*, **74**, 4471–4492.

Zucchini A., Petrelli M., Frondini F., Petrone C.M., Sassi P., Di Michele A., Palmerini S., Trippella O. and Busso M (2018) Chemical and mineralogical characterization of the Mineo (Sicily, Italy) pallasite: A unique sample. *Meteoritics & Planetary Science*, **53**, 268–283.